

Nonlinear time-reversal interferometry with arbitrary quadratic collective-spin interaction

Zhiyao Hu,^{1,2,*} Qixian Li,^{1,*} Xuanchen Zhang,^{1,*} He-bin Zhang,¹ Long-Gang Huang,^{1,3} and Yong-Chun Liu^{1,4,†}

¹*State Key Laboratory of Low-Dimensional Quantum Physics,
Department of Physics, Tsinghua University, Beijing 100084, China*

²*School of Physics, Xi'an Jiaotong University, Xi'an 710049, China*

³*China Fire and Rescue Institute, Beijing 102202, China*

⁴*Frontier Science Center for Quantum Information, Beijing 100084, China*

(Dated: November 30, 2023)

Atomic nonlinear interferometry has wide applications in quantum metrology and quantum information science. Here we propose a nonlinear time-reversal interferometry scheme with high robustness and metrological gain based on the spin squeezing generated by arbitrary quadratic collective-spin interaction, which could be described by the Lipkin-Meshkov-Glick (LMG) model. We optimize the squeezing process, encoding process, and anti-squeezing process, finding that the two particular cases of the LMG model, one-axis twisting and two-axis twisting outperform in robustness and precision, respectively. Moreover, we propose a Floquet driving method to realize equivalent time reverse in the atomic system, which leads to high performance in precision, robustness, and operability. Our study sets a benchmark in achieving high precision and robustness in atomic nonlinear interferometry.

I. INTRODUCTION

Improving precision and system robustness is always the main task in quantum metrology and quantum sensing. Projection noise, originating from the quantum fluctuations in the measured populations, is a fundamental limitation for the improvement of precision [1–5]. To break through the limit, many-body entanglement is usually needed [6–16], while spin squeezing [1, 17] is a widely used method. Squeezed spin states (SSSs) possess good properties of reduced spin fluctuations in certain directions, thus having a variety of applications in high-precision measurements, and quantum information science [18–31].

Despite squeezed spin states having great properties in reducing projection noise for quantum metrology, in real experiments, the precision we could achieve is still greatly restricted by other various types of noises, including the detection noise. Under certain ranges of detection noise, the metrological gain using squeezed spin states will decrease excessively [32]. To address this problem, an echo-like scheme similar to nonlinear interferometry is proposed [33–42]. In this scheme, apart from the squeezing process and encoding process, a quasi-time-reverse evolution called Interaction-Based Readout (IBR) is added before detection, which will significantly improve the robustness of the system to the detection noise [32, 43–51]. The added reversal control will improve the robustness of the system to the detection noise. However, the previous studies mostly focus on IBR generated by one-axis twisting (OAT) [17, 32] and two-axis twisting (TAT) [17, 46], which are very special cases of collective-spin interaction.

Besides, introducing the IBR scheme will lead to a trade-off between precision and robustness, which is very important but seldom investigated. Moreover, most of the previous studies assume that there exists a time-reversal control, which is not always easy to implement in experiments.

In this article, we investigate the performance of the nonlinear interferometry with arbitrary quadratic collective-spin interaction and propose the optimal scheme for high precision and high robustness in quantum metrology with the atomic system. To improve the precision and robustness of the system, we find the optimal squeezing process, phase encoding process, and anti-squeezing process with different anisotropic parameters for quadratic interaction. Through both analytical and numerical analysis, we also demonstrate the highest precision and highest robustness could be achieved simultaneously for the TAT interaction. Moreover, we propose a Floquet driving method to achieve the equivalent time-reversal control, which is implementable for arbitrary quadratic collective-spin interaction. We also show that the method is robust to imperfect pulse from the Floquet driving according to numerical simulations.

The paper is organized as follows. In Sec. (II) we first explain how the nonlinear interferometry works, introducing our system model and optimizing the interferometer processes with quadratic collective-spin interaction, which can be described by the LMG model. In Sec. (III), we propose that we could generate equivalent time reversal by making use of Floquet driving. In Sec. (IV), we show that the method is robust to different kinds of noise, followed by the summary.

* These authors contributed equally to this work.

† ycliu@tsinghua.edu.cn

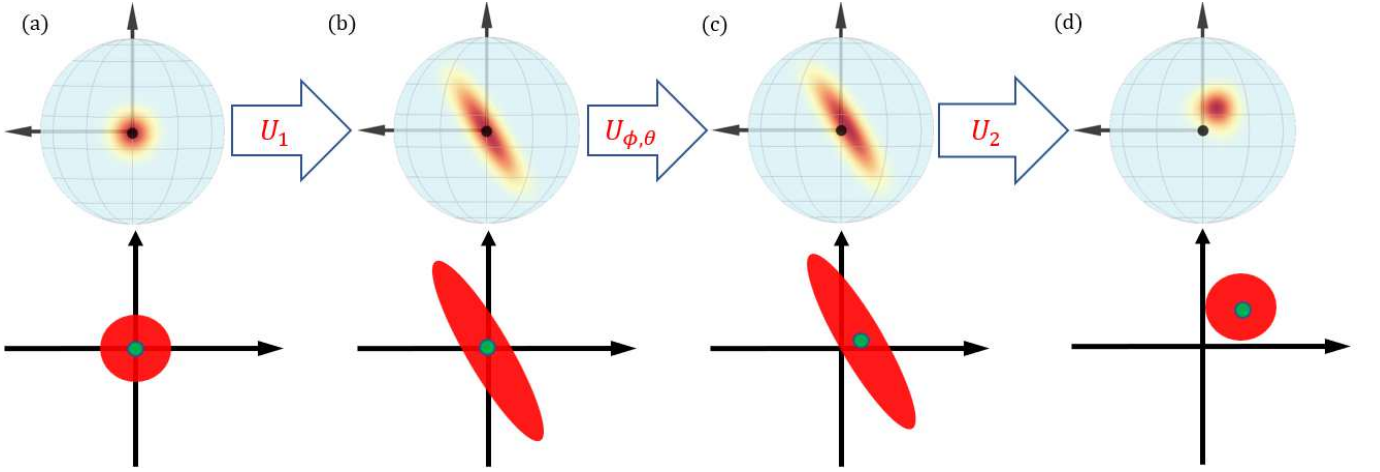


FIG. 1. The whole process of the (nonlinear) interferometry could be viewed as three steps. (i) A probe state (CSS) is prepared and it goes through the squeezing process U_1 . (ii) After the squeezing process U_1 , an unknown parameter ϕ is encoded into the state through $U_{\phi, \theta} = e^{-i\phi S_\theta}$ along S_θ , resulting in a small displacement in the Bloch Sphere. (iii) Then an anti-squeezing process U_2 is performed, which is immediately followed by the measurement. The schematic diagram of this process is shown in the bottom row.

II. SYSTEM MODEL AND NONLINEAR INTERFEROMETER SCHEME

As shown in Fig.1, the whole process of the nonlinear interferometer scheme could be viewed as three parts: First, a coherent spin state (CSS) is prepared and it evolves under U_1 for t_1 , in which the entanglement is generated and the state turns to squeezed or oversqueezed state. Following that is the encoding part, where the estimated value ϕ is encoded through $U_{\phi, \theta}$. After that comes the readout part, during which the squeezed spin state evolves under a time-reversed dynamics U_2 for t_2 , followed by a measurement. Now we consider how to optimize this scheme to achieve high precision and high robustness.

A. System model

Consider a system of mutually interacting spin-1/2 particles described by the following Hamiltonian:

$$H = \sum_{j,k} \chi_{\alpha\beta} \sigma_\alpha^j \sigma_\beta^k, \quad (1)$$

where σ_α^j is the Pauli operator of the j -th spin and $\alpha, \beta \in \{x, y, z\}$. The parameter $\chi_{\alpha\beta}$ characterizes the strength of the interaction in different directions. To ensure the Hermiticity of the Hamiltonian, we have $\chi_{\alpha\beta} = \chi_{\beta\alpha}$. Here we have the assumption that the interactions between individual spins are the same, and this assumption holds when there are all-to-all interactions, which is valid under some systems such as nuclear system [52], cavity QED [42], ion trap [53].

Now we introduce the collective spin operators $S_\alpha = \frac{\hbar}{2} \sum_j \sigma_\alpha^j$ with commutation relations $[S_\alpha, S_\beta] =$

$i\hbar \epsilon_{\alpha\beta\gamma} S_\gamma$, where α, β, γ denote the components in any three orthogonal directions, and $\epsilon_{\alpha\beta\gamma}$ is the Levi-Civita symbol, and we let $\hbar = 1$. H preserves the magnitude of the total spin $S^2 = \sum_\alpha S_\alpha^2$, namely, $[H, S^2] = 0$. By applying a linear transformation to the collective spin operators and redefining the coordinate axes we can prove that this Hamiltonian is equivalent to

$$H_{\text{LMG}}(\chi, \gamma) = \chi(S_x^2 + \gamma S_y^2), 0 \leq \gamma \leq 0.5 \quad (2)$$

which could be described as the Lipkin-Meshkov-Glick (LMG) model [52, 54]. In the expression of $H_{\text{LMG}}(\chi, \gamma)$, χ is the strength of the interaction which describes the rate at which the system evolved, and γ is the anisotropic parameter reflecting the symmetry of the system. OAT and TAT could be viewed as special cases when $\gamma = 0$ and $\gamma = 0.5$ [55].

B. Squeezing process

The first step of the nonlinear interferometer scheme is to generate entanglement. Consider a system with N interacting spin-1/2 particles, we choose a CSS as the initial state, which can be described by

$$|\vartheta, \varphi\rangle = e^{i\vartheta(S_x \sin \varphi - S_y \cos \varphi)} |j, j\rangle, \quad (3)$$

where ϑ is the angle between the z -axis and the collective-spin vector (polar angle), while φ is the angle between the x -axis and the vertical plane containing the collective-spin vector (azimuth angle). In the following, we set $\vartheta = \pi/2$ and $\varphi = \pi/2$, namely $|\hat{y}\rangle$, as the initial state.

Firstly, the system undergoes a unitary evolution U_1 , namely dynamics with the LMG Hamiltonian $H_{\text{LMG}}(\chi, \gamma)$ for t_1 in our strategy, evolving to a squeezed or oversqueezed state. For the system with different

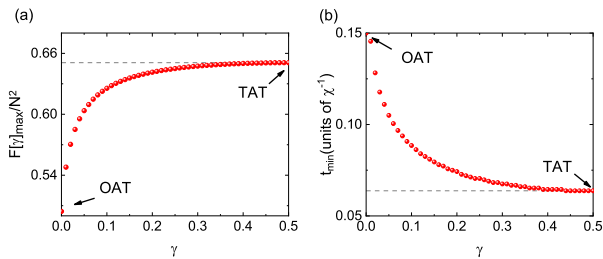


FIG. 2. (a) Maximum QFI for different anisotropic parameter γ with t_1 around the best squeezing time. (b) The corresponding t_1 to get $F[\gamma]_{\max}$ for different γ . The horizontal dashed lines correspond to the results of the TAT model (we choose the atom number $N = 100$).

anisotropic parameters γ , the corresponding t_1 to get the state with the highest precision varies as well. We need to optimize the evolution time t_1 in order to get the highest precision for estimating the value of the unknown parameter, which is bounded by quantum Cramer-Rao bound (QCRB) [56]:

$$(\Delta\phi)^2 \geq \frac{1}{kF[\rho_\lambda]}, \quad (4)$$

where k is the number of independent repetitions (in the following we set $k = 1$), and $F[\rho_\lambda]$ is the quantum Fisher information (QFI) [57–60] defined as:

$$F[\rho_\lambda] = \sum_{\kappa, \kappa'} \sum_{q_\kappa + q_{\kappa'} > 0} \frac{2}{q_\kappa + q_{\kappa'}} \left| \langle \kappa' | \partial_\lambda \rho_\lambda | \kappa \rangle \right|^2, \quad (5)$$

where $\hat{\rho}_\lambda = \sum_{\kappa} q_\kappa |\kappa\rangle \langle \kappa|$ is the λ -dependent density matrix and both the eigenvalues $q_\kappa \geq 0$ and the associated eigenvectors $|\kappa\rangle$ depend on λ , and λ is the known parameter to be estimated. For the system and parameterization we are interested in, as a pure state, the QFI simply becomes:

$$F[S_{\vec{n}}] = 4(\Delta S_{\vec{n}})^2, \quad (6)$$

where $S_{\vec{n}} = \sin \vartheta \cos \varphi S_x + \sin \vartheta \sin \varphi S_y + \cos \varphi S_z$. To set a higher bound for the precision of parameter estimation, t_1 should be set as the time realizing the highest QFI. For a certain γ , change the evolution time t'_1 and find the corresponding maximum QFI: $F[t'_1, \gamma]$. The maximum of $F[t'_1, \gamma]$ then is the largest QFI with this γ , denoted as $F[\gamma]_{\max}$, and the corresponding t'_1 is the t_1 . Now we change the γ , and track how $F[\gamma]_{\max}$ and t_1 changes when γ varies from 0 to 0.5.

The results are shown in Fig. 2. We find that $F[\gamma]_{\max}$ and t_1 monotonically depend on γ for $0 \leq \gamma \leq 0.5$. When $\gamma = 0.5$, the system attains its maximum $F[\gamma]_{\max}$, and the corresponding t_1 is also the shortest, corresponding to the TAT interaction. What is worth mentioning is that the range of t_1 we choose is around the best squeezing time, while the OAT interaction $H_{\text{OAT}} = \chi S_x^2$ could

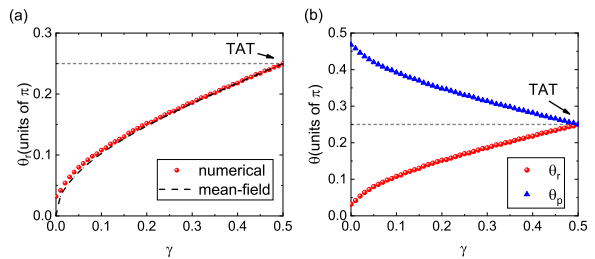


FIG. 3. (a) Numerical (red circle) and analytical results through mean-field approximation (black dashed line) of θ_r for different γ . (b) θ_r (red circle) and θ_p (blue triangle) for different γ . The horizontal short dashed lines correspond to the results of the TAT interaction ($N = 100$).

generate GHZ states at $t = \pi/2\chi$, the QFI of which could reach Heisenberg limit.

C. Encoding process

The entanglement of the system is generated through U_1 , followed by the application of the perturbation spin rotation $U_{\phi, \theta} = e^{-i\phi S_\theta}$, which also plays an important role in the nonlinear interferometry. Contrary to the traditional belief that the encoding part only has an effect on the precision so that the axis chosen to encode the parameter could simply choose the direction with minimum fluctuation, the encoding part has a vital influence on the robustness of the system to the detection noise if an anti-squeezing operator U_2 is applied before performing the measurement.

In our model, the squeezing happens in the x - z plane, so S_θ should be chosen in this plane to fully exploit the metrology-enhanced property. S_θ could be expressed as $S_\theta = S_x \sin \theta + S_z \cos \theta$, where θ is the angle between the z -axis and S_θ . The sensitivity for estimating ϕ and the robustness to detection noise of the system vary as θ takes different values. In the actual experiments, different measurements have different emphases. In some conditions, the precision might be the priority, while under certain circumstances the robustness against the measurement noise deserves extra attention. To quantify the robustness of the system to the detection noise, here we introduce the magnification factor G as:

$$G = \frac{\langle S_m^\phi \rangle}{\frac{N}{2} \cdot \phi}. \quad (7)$$

the numerator (denominator) represents the magnitude of the mean-spin measurement with (without) the time-reversal control, S_m is the spin component that we apply collective mean-spin measurement and m is a continuous parameter corresponding to an angle in the x - z plane, and G represents the phase magnification benefited from the time-reversed dynamics (here we assume that a perfect time-reversed dynamics is followed after the encoding

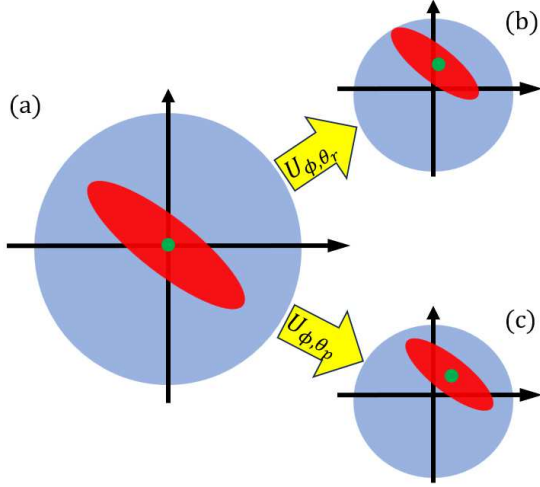


FIG. 4. After applying U_1 to the CSS, we get an SSS as the probe state. To encode the unknown parameter ϕ , $U_{\phi, \theta} = e^{-i\phi S_\theta}$ is applied to the SSS, and U_{ϕ, θ_r} (U_{ϕ, θ_p}) is chosen to encode the parameter, which maximizes the robustness (precision) of the process. (a) the SSS generated through U_1 . (b) the SSS after U_{ϕ, θ_r} . (c) the SSS after U_{ϕ, θ_p} .

process). A higher G indicates the influence of detection noise will have less influence on the signal, indicating the robustness to detection noise [32, 46].

We denote the corresponding θ as θ_r and θ_p with the directions that achieve the highest precision for estimation and robustness to detection noise, respectively. As γ changes, θ_r and θ_p would change as well. The analytical solution of the dependence of θ_r and θ_p with respect to γ is too complex to conduct, but we can give a brief and reasonably accurate estimate of θ_r . We use mean-field approximation to describe the time evolution after the parameter is encoded. The detail is shown in Appendix A. The calculation results in a brief expression of θ_r :

$$\theta_r = \arcsin \sqrt{\gamma}, \quad (8)$$

which has been proved to have enough accuracy when γ is not too small. The comparison of the numerical solution and mean-field results is shown in Fig. 3(a). We can see that our approximation is accurate enough, especially when γ approaches 0.5. When $\gamma = 0.5$, θ_r becomes $\pi/4$, which is consistent with previous research [46].

To get the estimated value of θ_p , we perform the numerical analysis by calculating the fluctuation for each θ after U_1 and finding the minimum one, taking the corresponding θ as θ_p for this γ . The result is shown in Fig. 3(b). Compared to θ_r , we show that for a certain γ , the corresponding θ_r and θ_p have an approximate relationship:

$$\theta_r + \theta_p \approx \pi/2. \quad (9)$$

We find that $\gamma = 0.5$ is a special situation when θ_r and θ_p take the same value $\pi/4$, which indicates that for the

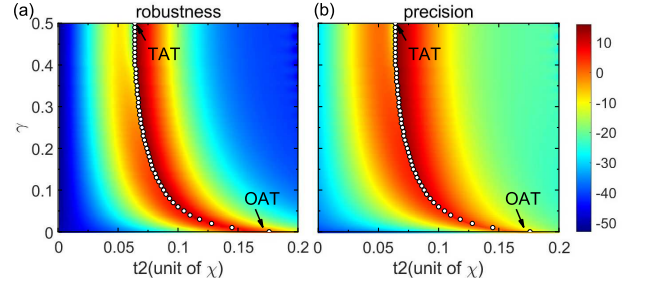


FIG. 5. ΔG as a function of t_2 , γ and θ , and here θ is chosen to optimize (a) robustness. (b) precision. The white dots represent optimal t_1 with $0 \leq \gamma \leq 0.5$.

TAT interaction, we can achieve the best robustness and precision simultaneously by setting $S_\theta = \frac{\sqrt{2}}{2}S_x + \frac{\sqrt{2}}{2}S_z$.

D. Anti-squeezing process

The time-reversed nonlinear dynamics is the key to our strategy. Applying $H_{\text{LMG}}(-\chi, \gamma)$ for t_2 , we could perform the anti-squeezing process to get the final state to measure. An appropriate t_2 is important in this step. To determine the optimal t_2 to achieve higher precision, we define the metrological gain as ΔG to investigate the effect of U_2 for t_2 [49]:

$$\Delta G = -20 \lg \left\{ \frac{\Delta \phi}{(\Delta \phi)_{\text{SQL}}} \right\}, \quad (10)$$

where $(\Delta \phi)_{\text{SQL}} = 1/\sqrt{N}$ is the standard quantum limit (SQL) [61] and $\Delta \phi$ is given by error propagation formula:

$$\Delta \phi = \left[\frac{\Delta S_m^\phi}{\partial_\phi \langle S_m^\phi \rangle} \right]_{\phi=0}, \quad (11)$$

where ΔS_m^ϕ is the standard deviation of S_m and $\partial_\phi = d/d\phi$. $\partial_\phi \langle S_m^\phi \rangle$ can be replaced by its first order approximation with respect to ϕ :

$$\begin{aligned} \langle S_m^\phi \rangle &= \langle \mathbf{y} | U_1^\dagger U_{\phi, \theta}^\dagger U_2^\dagger S_m U_2 U_{\phi, \theta} U_1 | \mathbf{y} \rangle \\ &= \langle \mathbf{y} | U_1^\dagger e^{iS_\theta \phi} U_2^\dagger S_m U_2 e^{-iS_\theta \phi} U_1 | \mathbf{y} \rangle \\ &= i\phi \langle \mathbf{y} | [S_\theta(U_1), S_m(U_2 U_1)] | \mathbf{y} \rangle + O(\phi^2), \end{aligned} \quad (12)$$

where we define $S(U) = U^\dagger S U$ for brevity.

Previously we proposed two directions of S_θ , and the dependence of metrological gain on t_2 and γ with different directions of S_θ is shown in Fig. 5, respectively. We show that with γ ranging from 0 to 0.5, to reach the maximum metrological gain, the time t_2 could always be chosen near $t_2 = t_1$, which is conducive for us to determine the reverse time t_2 for convenience. Besides, we find that TAT outperforms OAT in precision with the reversed dynamics when the unknown parameter is encoded through the axis of S_{θ_r} and S_{θ_p} , which is consistent with the previous study [46].

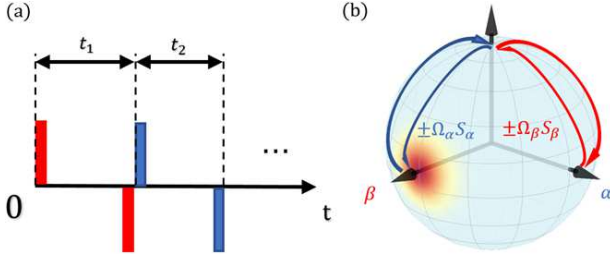


FIG. 6. (a) An illustration of the pulse sequences. The overall process could be viewed as the repetition of (a). The red(blue) -up(down) pulse represents a $+\pi/2(-\pi/2)$ pulse along the $\alpha(\beta)$ axis. (b) The pulse method could also be viewed as the cyclic rotation around the α and β axis on the Bloch sphere.

III. GENERATION OF EQUIVALENT TIME REVERSE

Realizing the interaction-based readout scheme requires implementable time-reversal control, which is usually not a trivial task in experiments. Inspired by the previous study, we propose that we could realize equivalent time reversal by making use of multiple $\pi/2$ pulses, which can be realized using the coupling term $\Omega_\alpha S_\alpha$ ($\alpha = x, y, z$) [54, 62, 63]. By making use of a multi-pulse sequence along the α -axis ($\alpha = x, y, z$), we can rotate the spin along the α -axis and affect the dynamic of squeezing. A $\pi/2$ pulse corresponds to $\int_{-\infty}^{+\infty} \Omega_\alpha(t) dt = \pi/2$, which leads to the result that $R_{\alpha, -\pi/2} e^{it\chi S_\beta^2} R_{\alpha, \pi/2} = e^{it\chi S_\alpha^2}$, where $R_{\alpha, \theta} = e^{-i\theta S_\alpha}$ and κ is the axis that perpendicular to the α -axis and β -axis. The multi-pulse sequence is periodic, and the frequency is determined by γ and the axis we choose.

To generate equivalent time reversal $U_2 = e^{iH_{\text{LMG}}t}$, one way is to generate $H = -H_{\text{LMG}} + kS^2$ since $[H, S^2] = 0$, the total spin will not have an effect on the squeezing properties while k is any constant. The whole time reversal process could be viewed as the repetitions of Fig.6 (a), and each period is made up of the following: a $-\pi/2$ pulse along the α -axis, a free evolution for t_1 , a $\pi/2$ along the α -axis, a $-\pi/2$ along the β -axis, a free evolution for t_2 , and a $\pi/2$ along the β -axis. The period is $t_c = t_1 + t_2$, neglecting the time needed for applying the four $\pi/2$ pulses. Fig.6(b) shows that the cyclic $\pm\pi/2$ could be viewed as rotations on the Bloch sphere. By adjusting the relationship between t_1 and t_2 , we can transform the LMG interaction into equivalent time-reversed dynamics.

One potential strategy to generate time reversal is to apply multiple pulses along the y -axis and z -axis. For $H_{\text{LMG}} = \chi(S_x^2 + \gamma S_y^2)$, with the y -axis to be the α -axis and z -axis to be the β -axis, the time evolution operates for a single period could be expressed as:

$$\begin{aligned} U_{yz} &= R_{y, -\pi/2} e^{-i(S_x^2 + \gamma S_y^2)\chi t_1} R_{y, \pi/2} \\ &R_{z, -\pi/2} e^{-i(S_x^2 + \gamma S_y^2)\chi t_2} R_{z, \pi/2} \\ &= e^{-i(S_x^2 + \gamma S_y^2)\chi t_1} e^{-i(S_y^2 + \gamma S_x^2)\chi t_2}. \end{aligned} \quad (13)$$

Using the Baker-Campbell-Hausdorff formula, we find $U_{yz} \approx e^{-i\chi[S_x^2(\gamma t_2) + S_y^2(\gamma t_1 + t_2) + S_z^2(t_1)]}$ for small t_1 and t_2 [64]. In order to achieve equivalent time reverse, the relationship between γ and t_2/t_1 should satisfy

$$\frac{t_2}{t_1} = \frac{1 - 2\gamma}{(1 - \gamma)(1 + \gamma)}. \quad (14)$$

Accordingly, we obtain the effective Hamiltonian

$$H_{yz}^{\text{eff}} = \frac{\chi_{\text{eff}}}{\chi} H_{\text{LMG}} = -\frac{\chi(\gamma^2 - \gamma + 1)}{-\gamma^2 - 2\gamma + 2} (S_x^2 + \gamma S_y^2), \quad (15)$$

With the anisotropic parameter γ ranging from 0 to 0.5, $\chi_{\text{eff}} = -\frac{(\gamma^2 - \gamma + 1)}{-\gamma^2 - 2\gamma + 2} < 0$, which means that we can generate equivalent time reverse by applying pulse sequences along the y -axis and z -axis.

IV. NOISE ANALYSIS

Now we analyze the performance of the time-reversal interferometry scheme under various kinds of noises, and here we focus on analyzing the impact of detection noise as well as the imperfect pulse. The former could be weakened by applying the time-reversal control, while the latter is introduced by the multiple pulse sequences involved in our scheme.

A. Detection noise

The effect of detection noise can be described by the measuring operator \hat{M} :

$$\hat{M} = \sum_{m, m'} \Gamma_{m, m'} |m'\rangle \langle m|, \quad (16)$$

where $|m\rangle$ is the m th eigen state of S_z and

$$\Gamma_{m, m'} = \frac{e^{-(m-m')^2/(2\sigma)^2}}{\sum_{m'} e^{-(m-m')^2/(2\sigma)^2}}, \quad (17)$$

determined by parameter σ . This setup means if the system is in $|m\rangle$ state, execute the measurement and there exists a probability of $\Gamma_{m, m'}$ to mistake $|m\rangle$ for $|m'\rangle$. $\Gamma_{m, m'}$ has a form of Gaussian convolution, which makes sense experimentally and mathematically. Now we define noise strength $\mathcal{N} = e^{-1/(2\sigma)^2}$, \hat{M} then could be expressed as:

$$\hat{M} = \frac{1}{1 + 2 \sum_n \mathcal{N}^{n^2}} \sum_{0 \leq m \pm k, 1 \leq m \leq N+1} \mathcal{N}^{k^2} |m \pm k\rangle \langle m| \quad (18)$$

\hat{M} could be regarded as a identity operator \hat{I} attached by higher order term of \mathcal{N} , which would cause a correction term in the angular sensitivity $\Delta\phi$. Now we define the robustness coefficient R as:

$$R = -\lg \frac{\partial \Delta\phi}{\partial \mathcal{N}}, \quad (19)$$

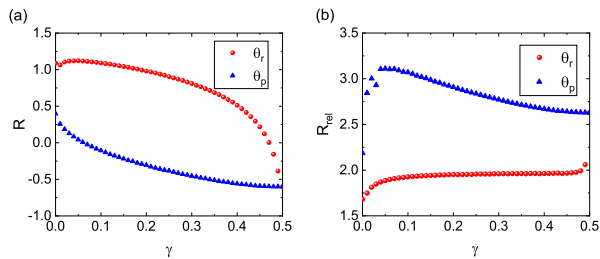


FIG. 7. (a) Under the noise strength $\mathcal{N} = 0.1$, the relationship between robustness coefficient R and θ_r , θ_p for different γ . (b) Under the noise strength $\mathcal{N} = 0.1$, the relative robustness coefficient R_{rel} with θ_r and θ_p for different γ compared to no time-reversed scheme. ($N = 100$).

which reflects the response of measurement results to the detection noise. A larger R means less response, namely better robustness. When \mathcal{N} is not too large (for example, $\mathcal{N} = 0.1$, which means a probability of 0.2 to make an error just in the detection procedure), we can get the value of R semi-analytically. For simplicity, we take $t_2 = t_1$. The detail is shown in Appendix B.

The conditions when S_θ is towards θ_r and θ_p are calculated respectively. The result is shown in Fig. 7(a). We can find that in most of the cases, the robustness is better when S_θ is towards θ_r . More precisely, when S_θ is towards θ_p , the additional fluctuation caused by detection noise is about 10 times as large as that of θ_r , especially when γ is small. When γ gets larger, this gap is narrowing. When $\gamma = 0.5$, the two curves coincide, for $\theta_r = \theta_p$ then.

In order to measure the noise suppression effect of our scheme, we also calculate the relative robustness coefficient: $R_{\text{rel}} = R - R_0$, where R_0 is the robustness coefficient when U_2 is Identity (no time-reversed dynamic is applied). The result is shown in Fig. 7(b). It can be concluded that for both θ_r and θ_p , the IBR method can reduce the effect of noise to 10^{-2} to 10^{-3} , which reflects the superiority of our scheme in noise reduction. Conversely, the R_{rel} of θ_p performs better than that of θ_r , and when $\gamma = 0.5$ it is the same as the two conditions.

B. Imperfect pulse

Apart from the detection noise, noise from imperfect pulses should also be taken into consideration. Firstly, our scheme assumes that the duration of each period is small enough to ignore the high-order term, which means the frequency for the pulse period is very high. Besides, the pulse area, pulse separation, and pulse phase are not always perfect. To verify the robustness of our scheme, we perform numerical simulations by adding Gaussian stochastic noises, i.e., assuming the fluctuating pulse areas, pulse separations and pulse phase are subject to Gaussian distribution with a standard deviation of different ranges of the average value.

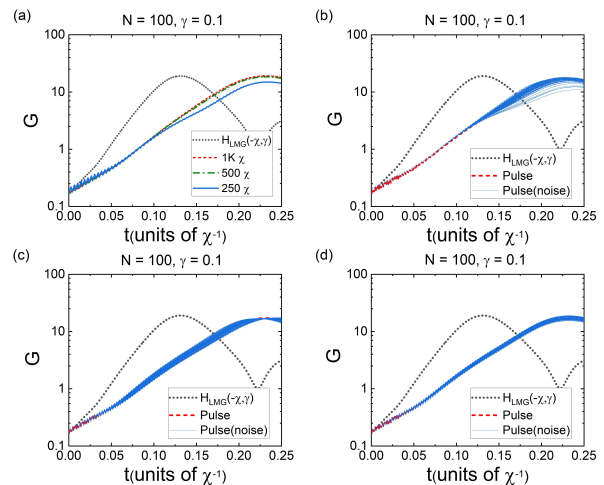


FIG. 8. Numerical analysis of the influence of noises for our scheme with $N = 100$, $\gamma = 0.1$. The blue curves crowding together denote the results of 100 independent simulations under different situations. (a) Evolution of the gain factor under different pulse frequencies. (b) Evolution of the gain factor G for 0.5% level of Gaussian stochastic noise adding on the pulse area. (c) Evolution of the gain factor G for 5% level of Gaussian stochastic noise adding on the pulse separation. (d) Evolution of the gain factor G for 0.1% level of Gaussian stochastic noise adding on the phase of the pulse.

To quantify the influence of imperfect pulse, As shown in Fig.8, by adding the noise into the pulse parameters and repeating the simulations 100 times, we show that under the circumstances that the noise of for pulse frequency higher than 500χ , noise in the pulse area less than 0.5%, noise in pulse separation less than 5%, and noise in pulse phase less than 0.1%, our method can almost achieve the optimal performance under perfect time reverse, indicating the robustness of the pulse scheme, and set the bound for experimentalists to realize the dynamics.

As for the spin decoherence, our method will not introduce new resources of decoherence but expend the experimental time, and we consider the situation that the coherence time is long enough to ignore the impact of spin decoherence [48], so we ignore the impact of extending the evolution time for spin decoherence for simplification.

V. SUMMARY

In summary, we investigate the performance of nonlinear time-reversal interferometry with quadratic collective-spin interaction. We design nonlinear interferometry based on that and optimize each part of this scheme with high precision and robustness with different anisotropic parameters. We find no tradeoffs in reaching the highest precision and robustness with the TAT interaction, which is an exceptional case in quadratic

collective-spin interaction, and we prove it through numerical and analytic analysis. Besides, we find that OAT outperforms in robustness while TAT outperforms in precision. To achieve the time reversal in this interferometry, we propose a Floquet-driving method to generate the equivalent time reversal. With $H_{\text{LMG}} = S_x^2 + \gamma S_y^2$, we find that by making use of multi-pulse sequences along y -axis and z -axis, we could achieve effective time reverse. We also show that our scheme is robust to different kinds of noise, including detection noise, and imperfect pulses. Our work will significantly deepen the insight of making use of atomic systems to achieve high precision and high robustness in nonlinear interferometry and push the frontier of quantum metrology.

VI. ACKNOWLEDGEMENT

We thank Guoqing Wang and Qi Liu for the helpful discussions. This work is supported by the National Key R&D Program of China (Grant No. 2023YFA1407600), and the National Natural Science Foundation of China (NSFC) (Grants No. 12275145, No. 92050110, No. 91736106, No. 11674390, and No. 91836302).

Appendix A: Mean-field approximation in perturbation encoding

For the LMG model, we have

$$[H, S^2] = 0, \quad (\text{A1})$$

which means $S^2 = S_x^2 + S_y^2 + S_z^2$ is constant during the evolution. Thus $H_{\text{LMG}}(\chi, \gamma)$ is equivalent to:

$$H_{\text{LMG}}(\chi, \gamma) - \chi\gamma S^2 = \chi[(1 - \gamma)S_x^2 - \gamma S_z^2]. \quad (\text{A2})$$

When the unknown parameter is encoded through S_θ , suppose S_α satisfies $S_\alpha = \langle S_\alpha \rangle + S_{\alpha 1}$, where $\alpha = x, z$ and $S_{\alpha 1}$ is the first order small quantity compared to S_α . Applying this approximation to Eqs. (A2), we can get the mean-field approximation of $H_{\text{LMG}}(\chi, \gamma)$:

$$H_{\text{LMG}}^{\text{mf}}(\chi, \gamma) = 2\chi[(1 - \gamma)\langle S_x \rangle S_x - \gamma\langle S_z \rangle S_z]. \quad (\text{A3})$$

For ϕ is far smaller than S , we can use S to represent $\langle S_y \rangle$. Consider $(\langle S_x \rangle, \langle S_z \rangle)$ as a point (x, z) on the phase plane. Applying Heisenberg equation to S_x and S_z , we have:

$$\begin{aligned} \frac{dx}{dt} &= \left\langle \frac{\partial S_x}{\partial t} \right\rangle \\ &= \left\langle \frac{1}{i\hbar} [S_x, H_{\text{LMG}}^{\text{mf}}] \right\rangle \\ &= 2\chi\gamma \langle S_y \rangle \langle S_z \rangle \\ &= 2\chi\gamma S z; \end{aligned} \quad (\text{A4})$$

$$\begin{aligned} \frac{dz}{dt} &= \left\langle \frac{\partial S_z}{\partial t} \right\rangle \\ &= \left\langle \frac{1}{i\hbar} [S_z, H_{\text{LMG}}^{\text{mf}}] \right\rangle \\ &= 2\chi(1 - \gamma) \langle S_y \rangle \langle S_x \rangle \\ &= 2\chi(1 - \gamma) S x, \end{aligned} \quad (\text{A5})$$

here we use the commutation relation of the collective spin operators:

$$[S_\alpha, S_\beta] = i\hbar \epsilon_{\alpha\beta\gamma} S_\gamma, \quad (\text{A6})$$

where α, β, γ denote the components in any three orthogonal directions, and $\epsilon_{\alpha\beta\gamma}$ is the Levi-Civita symbol. Combining Eqs. (A4) and Eqs. (A5), we get the evolution equation of x and z :

$$\begin{cases} \frac{d^2 x}{dt^2} = (2\chi S)^2 \gamma(1 - \gamma)x \\ \frac{d^2 z}{dt^2} = (2\chi S)^2 \gamma(1 - \gamma)z \end{cases}, \quad (\text{A7})$$

Solve the equations, we have

$$x = A e^{2\chi S \sqrt{\gamma(1-\gamma)}t} + B e^{-2\chi S \sqrt{\gamma(1-\gamma)}t} \quad (\text{A8})$$

$$z = C e^{2\chi S \sqrt{\gamma(1-\gamma)}t} + D e^{-2\chi S \sqrt{\gamma(1-\gamma)}t}, \quad (\text{A9})$$

where A, B, C, and D are undetermined coefficients. When $S_{\phi, \theta}$ has just added, we have:

$$\begin{cases} x_0 = S\phi \sin \theta \\ \left(\frac{dx}{dt}\right)_0 = 2S\chi\gamma z_0 = 2S^2\chi\gamma\phi \cos \theta \end{cases}, \quad (\text{A10})$$

apply which to Eqs. (A8) we can determine the expression for x :

$$\begin{aligned} x &= \frac{S\phi}{2} \left[\left(\sin \theta + \sqrt{\frac{\gamma}{1-\gamma}} \cos \theta \right) e^{2\chi S \sqrt{\gamma(1-\gamma)}t} \right. \\ &\quad \left. + \left(\sin \theta - \sqrt{\frac{\gamma}{1-\gamma}} \cos \theta \right) e^{-2\chi S \sqrt{\gamma(1-\gamma)}t} \right]. \end{aligned} \quad (\text{A11})$$

Similarly, we can get the expression for z :

$$\begin{aligned} z &= \frac{S\phi}{2} \left[\left(\sqrt{\frac{1-\gamma}{\gamma}} \sin \theta + \cos \theta \right) e^{2\chi S \sqrt{\gamma(1-\gamma)}t} \right. \\ &\quad \left. - \left(\sqrt{\frac{1-\gamma}{\gamma}} \sin \theta - \cos \theta \right) e^{-2\chi S \sqrt{\gamma(1-\gamma)}t} \right]. \end{aligned} \quad (\text{A12})$$

To ensure $\langle S_\phi \rangle$ reaches its maximum, we can equivalently ascertain a θ that makes the point (x, z) on the phase plane as far away from the origin as possible during the evolution. The distance from (x, z) to the origin is

$$\begin{aligned} \sqrt{x^2 + z^2} &= \frac{S\phi}{2} e^{2\chi S \sqrt{\gamma(1-\gamma)}t} \times \\ &\left[\left(\sqrt{\gamma} + \frac{1-\gamma}{\sqrt{\gamma}} \right) \sin \theta + \left(\sqrt{1-\gamma} + \frac{\gamma}{\sqrt{1-\gamma}} \right) \cos \theta \right], \end{aligned} \quad (\text{A13})$$

where we omit the terms with $e^{-2\chi S\sqrt{\gamma(1-\gamma)}t}$. Eqs. (A13) has maximum when

$$(\sqrt{\gamma} + \frac{1-\gamma}{\sqrt{\gamma}})\sin\theta + (\sqrt{1-\gamma} + \frac{\gamma}{\sqrt{1-\gamma}})\cos\theta \quad (\text{A14})$$

reaches its maximum, which leads to our result:

$$\theta_r = \arcsin\sqrt{\gamma}. \quad (\text{A15})$$

Appendix B: Semi-analytical solution of robustness coefficient R

When \mathcal{N} is not too large, the main source of error is mistaking $|m\rangle$ for $|m \pm 1\rangle$. The other term of \hat{M} would vanish because of the higher order of \mathcal{N} . Thus \hat{M} can be approximated by

$$\hat{M} \approx \frac{1}{1+2\mathcal{N}}(\hat{M}_0 + \mathcal{N}\hat{M}_1), \quad (\text{B1})$$

where \hat{M}_0 is simply the identity operator and $\hat{M}_1 = \sum_{m \in \mathbb{N}, m \pm 1 \geq 0} \mathcal{N} |m \pm 1\rangle \langle m|$. In matrix form, \hat{M}_0 can be denoted as an identity matrix I , and \hat{M}_1 can be denoted as a matrix M_1 with non-zero element $M_1(k, k+1) = M_1(k, k-1) = 1$. Taking M into consideration, the final state turns into: $MU_2 e^{-iS_\theta \phi} U_1 |\hat{\mathbf{y}}\rangle$. Applying Eqs. (B1) into Eqs. (12), we can get the expression of $\langle S_m^\phi \rangle$ under

the perturbation of \hat{M}_1 :

$$\begin{aligned} \langle S_m^\phi \rangle &= \langle \hat{\mathbf{y}} | U_1^\dagger U_{\phi, \theta}^\dagger U_2^\dagger M^\dagger S_m M U_2 U_{\phi, \theta} U_1 | \hat{\mathbf{y}} \rangle \\ &\approx \frac{1}{(1+2\mathcal{N})^2} \left\{ \langle \hat{\mathbf{y}} | U_1^\dagger e^{iS_\theta \phi} U_2^\dagger S_m U_2 e^{-iS_\theta \phi} U_1 | \hat{\mathbf{y}} \rangle \right. \\ &\quad \left. + \mathcal{N} \langle \hat{\mathbf{y}} | U_1^\dagger e^{iS_\theta \phi} U_2^\dagger \{M_1, S_m\} U_2 e^{-iS_\theta \phi} U_1 | \hat{\mathbf{y}} \rangle \right\} \\ &= \frac{i\phi}{(1+2\mathcal{N})^2} \left\{ \langle \hat{\mathbf{y}} | [S_\theta(U_1), S_m(U_2 U_1)] | \hat{\mathbf{y}} \rangle \right. \\ &\quad \left. + \mathcal{N} \langle \hat{\mathbf{y}} | [S_\theta(U_1), \{M_1, S_m\}(U_2 U_1)] | \hat{\mathbf{y}} \rangle \right\} \\ &\quad + O(\phi^2), \end{aligned} \quad (\text{B2})$$

where we define $\{M_1, S_m\} = M_1 S_m + S_m M_1$. Expanding to the first order of \mathcal{N} , then we can get an approximation of $\partial_\phi \langle S_m^\phi \rangle$:

$$\begin{aligned} \partial_\phi \langle S_m^\phi \rangle &= \frac{i}{(1+2\mathcal{N})^2} \left\{ \langle \hat{\mathbf{y}} | [S_\theta(U_1), S_m(U_2 U_1)] | \hat{\mathbf{y}} \rangle \right. \\ &\quad \left. + \mathcal{N} \langle \hat{\mathbf{y}} | [S_\theta(U_1), \{M_1, S_m\}(U_2 U_1)] | \hat{\mathbf{y}} \rangle \right\} \\ &\approx i \left\{ (1-4\mathcal{N}) \langle \hat{\mathbf{y}} | [S_\theta(U_1), S_m(U_2 U_1)] | \hat{\mathbf{y}} \rangle \right. \\ &\quad \left. + \mathcal{N} \langle \hat{\mathbf{y}} | [S_\theta(U_1), \{M_1, S_m\}(U_2 U_1)] | \hat{\mathbf{y}} \rangle \right\} \\ &\quad + O(\phi^2). \end{aligned} \quad (\text{B3})$$

Applying Eqs. (B3) to Eqs. (11) and expanding to the first order of \mathcal{N} , we can get the corrected $\Delta\phi$:

$$\frac{\partial \Delta\phi}{\partial \mathcal{N}} = \left[\frac{\Delta S_m^\phi}{\partial_\phi \langle S_m^\phi \rangle} \left\{ 4 - \frac{\langle \hat{\mathbf{y}} | [S_\theta(U_1), \{M_1, S_m\}(U_2 U_1)] | \hat{\mathbf{y}} \rangle}{\langle \hat{\mathbf{y}} | [S_\theta(U_1), S_m(U_2 U_1)] | \hat{\mathbf{y}} \rangle} \right\} \right]_{\phi=0}, \quad (\text{B4})$$

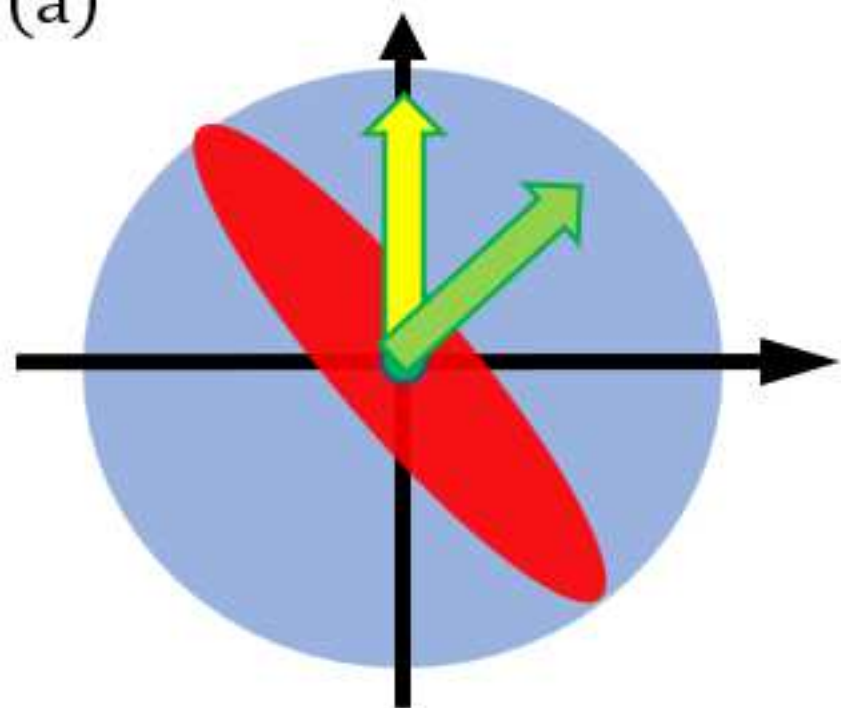
and go further to figure out R .

-
- [1] D. J. Wineland, J. J. Bollinger, W. M. Itano, and D. Heinzen, Squeezed atomic states and projection noise in spectroscopy, *Physical Review A* **50**, 67 (1994).
- [2] W. M. Itano, J. C. Bergquist, J. J. Bollinger, J. Gilligan, D. Heinzen, F. Moore, M. Raizen, and D. J. Wineland, Quantum projection noise: Population fluctuations in two-level systems, *Physical Review A* **47**, 3554 (1993).
- [3] G. Santarelli, P. Laurent, P. Lemonde, A. Clairon, A. G. Mann, S. Chang, A. N. Luiten, and C. Salomon, Quantum projection noise in an atomic fountain: A high stability cesium frequency standard, *Physical Review Letters* **82**, 4619 (1999).
- [4] A. Louchet-Chauvet, J. Appel, J. J. Renema, D. Oblak, N. Kjaergaard, and E. S. Polzik, Entanglement-assisted atomic clock beyond the projection noise limit, *New Journal of Physics* **12**, 065032 (2010).
- [5] Y.-C. Liu, K. Huang, Y.-F. Xiao, L. Yang, and C.-W. Qiu, What limits limits?, *National Science Review* **8**, nwaa210 (2021).
- [6] A. Sørensen, L.-M. Duan, J. I. Cirac, and P. Zoller, Many-particle entanglement with bose-einstein condensates, *Nature* **409**, 63 (2001).
- [7] L. Amico, R. Fazio, A. Osterloh, and V. Vedral, Entanglement in many-body systems, *Reviews of modern physics* **80**, 517 (2008).
- [8] R. Orús, S. Dusuel, and J. Vidal, Equivalence of critical scaling laws for many-body entanglement in the lipkin-meshkov-glick model, *Physical review letters* **101**, 025701 (2008).
- [9] R. Islam, R. Ma, P. M. Preiss, M. Eric Tai, A. Lukin, M. Rispoli, and M. Greiner, Measuring entanglement entropy in a quantum many-body system, *Nature* **528**, 77 (2015).
- [10] F. Reiter, D. Reeb, and A. S. Sørensen, Scalable dissipative preparation of many-body entanglement, *Physical review letters* **117**, 040501 (2016).
- [11] D. A. Abanin, E. Altman, I. Bloch, and M. Serbyn, Colloquium: Many-body localization, thermalization, and entanglement, *Reviews of Modern Physics* **91**, 021001 (2019).
- [12] E. Pedrozo-Peñafiel, S. Colombo, C. Shu, A. F. Adiyatullin, Z. Li, E. Mendez, B. Braverman, A. Kawasaki,

- D. Akamatsu, Y. Xiao, *et al.*, Entanglement on an optical atomic-clock transition, *Nature* **588**, 414 (2020).
- [13] X.-Y. Luo, Y.-Q. Zou, L.-N. Wu, Q. Liu, M.-F. Han, M. K. Tey, and L. You, Deterministic entanglement generation from driving through quantum phase transitions, *Science* **355**, 620 (2017).
- [14] A. S. Sørensen and K. Mølmer, Entanglement and extreme spin squeezing, *Physical Review Letters* **86**, 4431 (2001).
- [15] G.-R. Jin, Y.-C. Liu, and W.-M. Liu, Spin squeezing in a generalized one-axis twisting model, *New Journal of Physics* **11**, 073049 (2009).
- [16] Y. Liu, G. Jin, and L. You, Quantum-limited metrology in the presence of collisional dephasing, *Physical Review A* **82**, 045601 (2010).
- [17] M. Kitagawa and M. Ueda, Squeezed spin states, *Physical Review A* **47**, 5138 (1993).
- [18] C. L. Degen, F. Reinhard, and P. Cappellaro, Quantum sensing, *Reviews of modern physics* **89**, 035002 (2017).
- [19] Y.-Q. Zou, L.-N. Wu, Q. Liu, X.-Y. Luo, S.-F. Guo, J.-H. Cao, M. K. Tey, and L. You, Beating the classical precision limit with spin-1 dicke states of more than 10,000 atoms, *Proceedings of the National Academy of Sciences* **115**, 6381 (2018).
- [20] F. Yang, Y.-C. Liu, and L. You, Atom-photon spin-exchange collisions mediated by rydberg dressing, *Physical Review Letters* **125**, 143601 (2020).
- [21] M. Gärttner, J. G. Bohnet, A. Safavi-Naini, M. L. Wall, J. J. Bollinger, and A. M. Rey, Measuring out-of-time-order correlations and multiple quantum spectra in a trapped-ion quantum magnet, *Nature Physics* **13**, 781 (2017).
- [22] D. Braun, G. Adesso, F. Benatti, R. Floreanini, U. Marzolino, M. W. Mitchell, and S. Pirandola, Quantum-enhanced measurements without entanglement, *Reviews of Modern Physics* **90**, 035006 (2018).
- [23] H. Strobel, W. Muessel, D. Linnemann, T. Zibold, D. B. Hume, L. Pezzè, A. Smerzi, and M. K. Oberthaler, Fisher information and entanglement of non-gaussian spin states, *Science* **345**, 424 (2014).
- [24] V. Borish, O. Marković, J. A. Hines, S. V. Rajagopal, and M. Schleier-Smith, Transverse-field ising dynamics in a rydberg-dressed atomic gas, *Physical review letters* **124**, 063601 (2020).
- [25] Z. Li, B. Braverman, S. Colombo, C. Shu, A. Kawasaki, A. F. Adiyatullin, E. Pedrozo-Peñafiel, E. Mendez, and V. Vuletić, Collective spin-light and light-mediated spin-spin interactions in an optical cavity, *PRX Quantum* **3**, 020308 (2022).
- [26] R. Corgier, N. Gaaloul, A. Smerzi, and L. Pezzè, Delta-kick squeezing, *Physical Review Letters* **127**, 183401 (2021).
- [27] K. Gietka and H. Ritsch, Squeezing and overcoming the heisenberg scaling with spin-orbit coupled quantum gases, *Physical Review Letters* **130**, 090802 (2023).
- [28] L.-G. Huang, X. Zhang, Y. Wang, Z. Hua, Y. Tang, and Y.-C. Liu, Heisenberg-limited spin squeezing in coupled spin systems, *Physical Review A* **107**, 042613 (2023).
- [29] M. Gessner, A. Smerzi, and L. Pezzè, Metrological nonlinear squeezing parameter, *Physical review letters* **122**, 090503 (2019).
- [30] M. H. Muñoz-Arias, I. H. Deutsch, and P. M. Poggi, Phase-space geometry and optimal state preparation in quantum metrology with collective spins, *PRX Quantum* **4**, 020314 (2023).
- [31] F. Chen, J.-J. Chen, L.-N. Wu, Y.-C. Liu, and L. You, Extreme spin squeezing from deep reinforcement learning, *Physical Review A* **100**, 041801 (2019).
- [32] E. Davis, G. Bentsen, and M. Schleier-Smith, Approaching the heisenberg limit without single-particle detection, *Physical review letters* **116**, 053601 (2016).
- [33] B. Yurke, S. L. McCall, and J. R. Klauder, Su (2) and su (1, 1) interferometers, *Physical Review A* **33**, 4033 (1986).
- [34] W. N. Plick, J. P. Dowling, and G. S. Agarwal, Coherent-light-boosted, sub-shot noise, quantum interferometry, *New Journal of Physics* **12**, 083014 (2010).
- [35] Z. Ou, Enhancement of the phase-measurement sensitivity beyond the standard quantum limit by a nonlinear interferometer, *Physical Review A* **85**, 023815 (2012).
- [36] M. Gabbriellini, L. Pezze, and A. Smerzi, Spin-mixing interferometry with bose-einstein condensates, *Physical Review Letters* **115**, 163002 (2015).
- [37] F. Fröwis, P. Sekatski, and W. Dür, Detecting large quantum fisher information with finite measurement precision, *Physical review letters* **116**, 090801 (2016).
- [38] D. Linnemann, H. Strobel, W. Muessel, J. Schulz, R. J. Lewis-Swan, K. V. Kheruntsyan, and M. K. Oberthaler, Quantum-enhanced sensing based on time reversal of nonlinear dynamics, *Physical Review Letters* **117**, 013001 (2016).
- [39] S. S. Szigeti, R. J. Lewis-Swan, and S. A. Haine, Pumped-up su (1, 1) interferometry, *Physical Review Letters* **118**, 150401 (2017).
- [40] Z. Ou and X. Li, Quantum su (1, 1) interferometers: Basic principles and applications, *APL Photonics* **5**, 080902 (2020).
- [41] Q. Liu, L.-N. Wu, J.-H. Cao, T.-W. Mao, X.-W. Li, S.-F. Guo, M. K. Tey, and L. You, Nonlinear interferometry beyond classical limit enabled by cyclic dynamics, *Nature Physics* **18**, 167 (2022).
- [42] S. Colombo, E. Pedrozo-Peñafiel, A. F. Adiyatullin, Z. Li, E. Mendez, C. Shu, and V. Vuletić, Time-reversal-based quantum metrology with many-body entangled states, *Nature Physics* **18**, 925 (2022).
- [43] T. Macrì, A. Smerzi, and L. Pezzè, Loschmidt echo for quantum metrology, *Physical Review A* **94**, 010102 (2016).
- [44] S. P. Nolan, S. S. Szigeti, and S. A. Haine, Optimal and robust quantum metrology using interaction-based readouts, *Physical Review Letters* **119**, 193601 (2017).
- [45] S. A. Haine, Using interaction-based readouts to approach the ultimate limit of detection-noise robustness for quantum-enhanced metrology in collective spin systems, *Physical Review A* **98**, 030303 (2018).
- [46] F. Anders, L. Pezzè, A. Smerzi, and C. Klempt, Phase magnification by two-axis countertwisting for detection-noise robust interferometry, *Physical Review A* **97**, 043813 (2018).
- [47] M. Schulte, V. J. Martínez-Lahuerta, M. S. Scharnagl, and K. Hammerer, Ramsey interferometry with generalized one-axis twisting echoes, *Quantum* **4**, 268 (2020).
- [48] Z. Li, S. Colombo, C. Shu, G. Velez, S. Pilatowsky-Cameo, R. Schmied, S. Choi, M. Lukin, E. Pedrozo-Peñafiel, and V. Vuletić, Improving metrology with quantum scrambling, *arXiv preprint arXiv:2212.13880* (2022).

- [49] Q. Liu, T.-W. Mao, M. Xue, L.-N. Wu, and L. You, Cyclic nonlinear interferometry with entangled non-gaussian spin states, *Physical Review A* **107**, 052613 (2023).
- [50] S. S. Mirkhalaf, S. P. Nolan, and S. A. Haine, Robustifying twist-and-turn entanglement with interaction-based readout, *Physical Review A* **97**, 053618 (2018).
- [51] J. Huang, M. Zhuang, B. Lu, Y. Ke, and C. Lee, Achieving heisenberg-limited metrology with spin cat states via interaction-based readout, *Physical Review A* **98**, 012129 (2018).
- [52] H. J. Lipkin, N. Meshkov, and A. Glick, Validity of many-body approximation methods for a solvable model:(i). exact solutions and perturbation theory, *Nuclear Physics* **62**, 188 (1965).
- [53] J. G. Bohnet, B. C. Sawyer, J. W. Britton, M. L. Wall, A. M. Rey, M. Foss-Feig, and J. J. Bollinger, Quantum spin dynamics and entanglement generation with hundreds of trapped ions, *Science* **352**, 1297 (2016).
- [54] Z. Hu, Q. Li, X. Zhang, L.-G. Huang, H.-b. Zhang, and Y.-C. Liu, Spin squeezing with arbitrary quadratic collective-spin interactions, *Phys. Rev. A* **108**, 023722 (2023).
- [55] One general Hamiltonian for the TAT interaction is $H_{\text{TAT}} = S_x S_y + S_y S_x$ for $\theta = \pi/2$ $\phi = \pm\pi/4$. By changing the initial states and twisting axes, the TAT interaction could also be expressed as $H_{\text{TAT}} = S_x^2 - S_z^2$. While the constant of $S^2 = S_x^2 + S_y^2 + S_z^2$ will not influence the properties of spin squeezing, we simply ignore it, and that makes the TAT interaction as $H_{\text{TAT}} = 0.5(S_x^2 - S_z^2)$.
- [56] S. L. Braunstein and C. M. Caves, Statistical distance and the geometry of quantum states, *Physical Review Letters* **72**, 3439 (1994).
- [57] R. A. Fisher, Theory of statistical estimation, in *Mathematical proceedings of the Cambridge philosophical society*, Vol. 22 (Cambridge University Press, 1925) pp. 700–725.
- [58] S. L. Braunstein, C. M. Caves, and G. J. Milburn, Generalized uncertainty relations: theory, examples, and lorentz invariance, *annals of physics* **247**, 135 (1996).
- [59] V. Giovannetti, S. Lloyd, and L. Maccone, Quantum metrology, *Physical review letters* **96**, 010401 (2006).
- [60] V. Giovannetti, S. Lloyd, and L. Maccone, Advances in quantum metrology, *Nature photonics* **5**, 222 (2011).
- [61] V. Giovannetti, S. Lloyd, and L. Maccone, Quantum-enhanced measurements: beating the standard quantum limit, *Science* **306**, 1330 (2004).
- [62] Y. Liu, Z. Xu, G. Jin, and L. You, Spin squeezing: transforming one-axis twisting into two-axis twisting, *Physical review letters* **107**, 013601 (2011).
- [63] X. Zhang, Z. Hu, and Y.-C. Liu, Fast generation of ghz-like states using collective-spin xyz model, *arXiv preprint arXiv:2311.04560* (2023).
- [64] The BCH formula has the expression as $e^A e^B = \exp(A + B + \frac{1}{2!}[A, B] + \frac{1}{3!}(\frac{1}{2!}[A, [A, B]] + \frac{1}{2!}[[A, B], B] + \dots))$.

(a)



(b)

